ACS NANO

www.acsnano.org

ARTICLE

High-Performance All-Inorganic Solid-State Sodium–Sulfur Battery

Jie Yue,[†,‡] Fudong Han,[†] Xiulin Fan,[†] Xiangyang Zhu,[†] Zhaohui Ma,[†] Jian Yang,[*,‡] and Chunsheng Wang[*,†]

[†]Department of Chemical and Biomolecular Engineering, University of Maryland, College Park, Maryland 20742, United States

[‡]Key Laboratory of Colloid and Interface Chemistry, Ministry of Education, School of Chemistry and Chemical Engineering, Shandong University, Jinan 250100, P.R. China

Supporting Information

ABSTRACT: **All-inorganic solid-state sodium–sulfur batteries (ASSBs) are promising technology for stationary energy storage due to their high safety, high energy, and abundant resources of both sodium and sulfur. However, current ASSB shows poor cycling and rate performances mainly due to the huge electrode/electrolyte interfacial resistance arising from the insufficient triple-phase contact among sulfur active material, ionic conductive solid electrolyte, and electronic conductive carbon. Herein, we report an innovative approach to address the interfacial problem using a Na_3PS_4–Na_2S–C (carbon) nanocomposite as the cathode for ASSBs. Highly ionic conductive Na_3PS_4 contained in the nanocomposite can function as both solid electrolyte and active material (catholyte) after mixing with electronic conductive carbon, leading to an intrinsic superior electrode/electrolyte interfacial contact because only a two-phase contact is required for the charge transfer reaction. Introducing nanosized Na_2S into the nanocomposite cathode can effectively improve the capacity. The homogeneous distribution of nanosized Na_2S, Na_3PS_4, and carbon in the nanocomposite cathode could ensure a high mixed (ionic and electronic) conductivity and a sufficient interfacial contact. The Na_3PS_4-nanosized Na_2S–carbon nanocomposite cathode delivered a high initial discharge capacity of 869.2 mAh g^{-1} at 50 mA g^{-1} with great cycling and rate capabilities at 60 °C, representing the best performance of ASSBs reported to date and therefore constituting a significant step toward high-performance ASSBs for practical applications.**

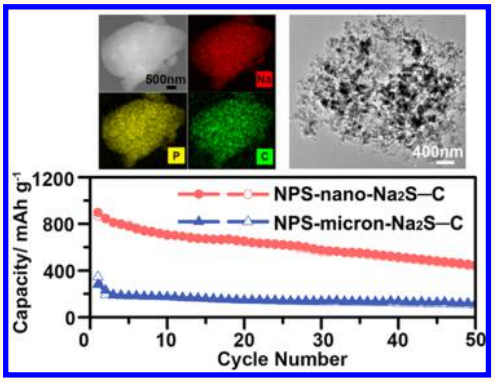

KEYWORDS: *nanocomposite, electrode design, all-inorganic, all-solid-state, sodium–sulfur battery*

Sodium–sulfur (Na–S) batteries have been considered as a promising technology for stationary energy storage due to the intrinsically high capacities of sodium and sulfur electrodes and their abundant resources.[1−4] The traditional Na–S battery operates at a high temperature (>300 °C) with β-alumina as solid electrolyte and liquid sodium (T_m = 98 °C) and sulfur (T_m = 115 °C) as electrodes.[2−4] During operation, the electrodes have to be in the molten state, meaning that only Na_2S_x species with low melting points are allowed to be formed during the sodiation (discharge) process. As a result, only one-third utilization of theoretical capacity of sulfur can be achieved in this system because the formation of Na_2S_2 and Na_2S upon sodiation could not be realized due to the high melting point of Na_2S_2 (T_m = 470 °C) and Na_2S (T_m = 1168 °C). In addition, the operation of the reactive, corrosive molten electrodes could induce a series of technical challenges in terms of safety, materials cost, high-temperature sealing and reliability, *etc.*[2−4] In order to address these issues, low-temperature Na–S batteries using organic liquid[1,5−12] or polymer electrolytes[13,14] have been developed. Despite great improvement on the utilization of sulfur, the safety concerns arising from the flammable organic electrolytes,[15,16] the shuttle reaction due to the dissolution of sodium polysulfides,[17] and the formation of the sodium dendrite during cycling are the main obstacles toward their practical applications.[18] The ultimate solution for these issues lies into the development of a low-temperature all-inorganic solid-state sodium–sulfur battery (ASSB) because the nonflammable inorganic solid electrolytes could eliminate the dissolution of sodium polysulfides and suppress the dendrite formation.[19,20] Despite these great promises, the performance of the ASSBs was largely limited by the huge electrode/electrolyte interfacial resistance. To date, there is only one report on the ASSB using Na_2S–P_2S_5 glass as solid electrolyte, commercialized micron-sized sulfur (mixed with solid electro-

Received: February 28, 2017
Accepted: May 1, 2017
Published: May 1, 2017

DOI: 10.1021/acsnano.7b01445
ACS Nano 2017, 11, 4885–4891

lyte and activated carbon) as cathode, and Na−Sn alloy as anode.[20] However, the cell could only cycle two times, and its rate capability is much lower than that of the conventional liquid or polymer electrolyte sodium−sulfur batteries.

The huge interfacial resistance in ASSB mainly results from the electronic and ionic insulating nature of the sulfur electrode and its discharge product. In the liquid electrolyte Na−S battery, only the electronic conductivity of the cathode should be ensured because the flowable and infiltrative liquid electrolyte and the dissolved high-order polysulfide catholyte could provide sufficient ionic conductivity.[11,21−23] However, a high-performance ASSB can only be realized if sulfur active material, solid electrolyte, and carbon are homogeneously distributed in the cathode with sufficient triple-phase contact for charge transfer reaction. The high rate performance of the catholyte in the liquid electrolyte Na−S battery inspired us and another group to use lithium-conducting sulfide electrolyte as the cathodes (catholytes) in solid-state battereis.[24−26] Utilization of lithium-conducting solid electrolyte as the electrode demonstrated a great advantage in improving the interfacial contact in the solid-state battery cathode because only a two-phase contact (between solid electrolyte and carbon) is required instead. However, the excellent cycling and rate performances of electrolyte/carbon catholyte were achieved with a sacrifice of energy density because of the high mass of the inactive components contained in the electrolyte. How to effectively improve the specific capacity while maintaining a high ionic/electronic conductivity of the sulfur cathode is very important for the development of high-performance ASSBs.

Herein, we report a Na_3PS_4−Na_2S−C nanocomposite cathode for ASSB wherein Na-ion conductive Na_3PS_4 functions as both solid electrolyte and active material (catholyte), and nanosized Na_2S is also an active material to further enhance the energy density of the battery. The uniform distribution of Na_3PS_4 and Na_2S in a nanoscale carbon matrix ensures sufficient interfacial contact while maintaining high ionic/electronic conductivities of the cathode.[19,27−29] Utilization of the pre-expanded Na_2S-based active materials could allow the utilization of sodium-free anode and, more importantly, provide enough space for the volume change of the solid electrode during charge/discharge.[19] The nanosized active material can also shorten the diffusion paths for both Na^+ and electrons, which will further increase the utilization of the active material during charge and discharge processes.[27] In addition, a nanocomposite electrode with enhanced mechanical property could also help accommodate the volume change of the electrode during charge/discharge.[19] With these advantages, the Na_3PS_4−Na_2S−C nanocomposite cathode exhibited an extremely high electrochemical performance in the all-inorganic Na−Sn−C/Na_3PS_4/Na_3PS_4−Na_2S−C battery.

RESULTS AND DISCUSSION

Figure 1a shows the XRD pattern of as-synthesized Na_3PS_4 (NPS) solid electrolyte. All the peaks can be well indexed to (110), (200), (211), (220), (310), (222), (321), (330), (420), (422), and (431) of cubic Na_3PS_4. The broad peak at around 18° is ascribed to the airtight sample holder for the XRD test. Figure 1 b,c shows the XRD patterns of the Na_3PS_4−C (NPS−C) catholyte and Na_3PS_4-nanosized Na_2S−C (NPS-nano-Na_2S−C) nanocomposite cathode, which were prepared by ball-milling method. The nanosized Na_2S in the NPS-nano-Na_2S−C nanocomposite was fabricated by ball-milling the commercialized Na_2S (Figure S1a). No impurities could be

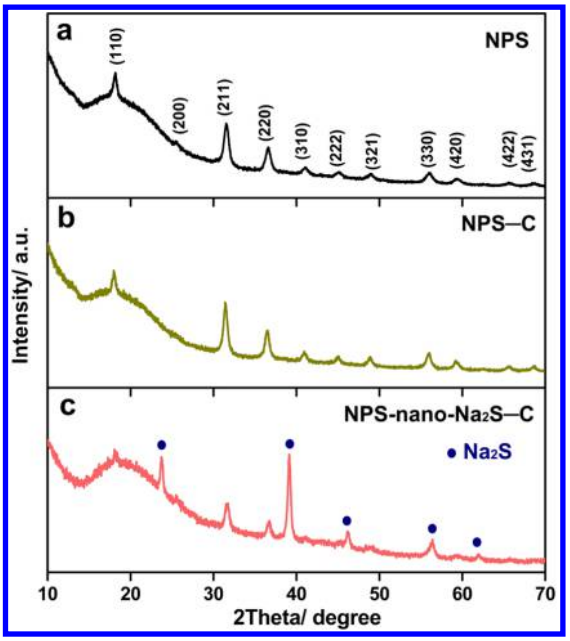

Figure 1. XRD patterns of NPS solid electrolyte (a), NPS−C catholyte (b), and NPS-nano-Na_2S−C nanocomposite cathode (c).

observed from the XRD patterns of the NPS−C catholyte and NPS-nano-Na_2S−C nanocomposite cathode, indicating their great stability during the ball-milling process. In addition, the Na_3PS_4-micron-sized Na_2S−C (NPS-micron-Na_2S−C) composite was also prepared as a control cathode by ball-milling Na_3PS_4 and acetylene black with commercial micron-sized Na_2S (Figure S1b). The weight ratio of Na_3PS_4, Na_2S, and C in the NPS-nano-Na_2S−C and NPS-micron-Na_2S−C composites are kept the same (50:25:25).

Figure 2a shows the scanning electron microscopy (SEM) image of the as-synthesized NPS solid electrolyte. The particle size of the NPS electrolyte is around 1−3 μm. The SEM image of the NPS−C catholyte is shown in Figure S2. After ball-milling with acetylene black, the particle size of NPS was largely reduced to around 200 nm. In addition, the uniform elemental distributions of Na, P, and C (Figure S2) confirmed the homogeneous mixing of NPS with carbon. Figure 2b displays the SEM image of Na_2S active material prepared by ball-milling the commercial Na_2S, and the particle size of the Na_2S was reduced from several microns (Figure S3a) to around 200 nm. The SEM image and elemental mappings of the NPS-nano-Na_2S−C nanocomposite are shown in Figure 2c. Very uniform distributions of sodium, phosphorus, and carbon in the sample demonstrates that Na_2S, Na_3PS_4, and C are homogeneously distributed in the NPS-nano-Na_2S−C nanocomposite electrode. Transmission electron microscopy (TEM) image of the NPS-nano-Na_2S−C nanocomposite (Figure 2d) shows that the large particle observed in Figure 2c is actually composed of a large amount of small particles with the particles size around tens of nanometers, confirming the formation of NPS-nano-Na_2S−C nanocomposites. On the other hand, the Na_3PS_4-micron-Na_2S−C composite consists of irregular particles with particle sizes from nanometers to several microns, as shown in Figure S3b−f. The large particles (shown in Figure S3b) in the NPS-micron-Na_2S−C composite have large contents of the Na but no P, which implies that these large particles are mainly micron-sized Na_2S. Additionally, neither phosphorus nor carbon was uniformly coated on these particles, indicating the

DOI: 10.1021/acsnano.7b01445
ACS Nano 2017, 11, 4885−4891

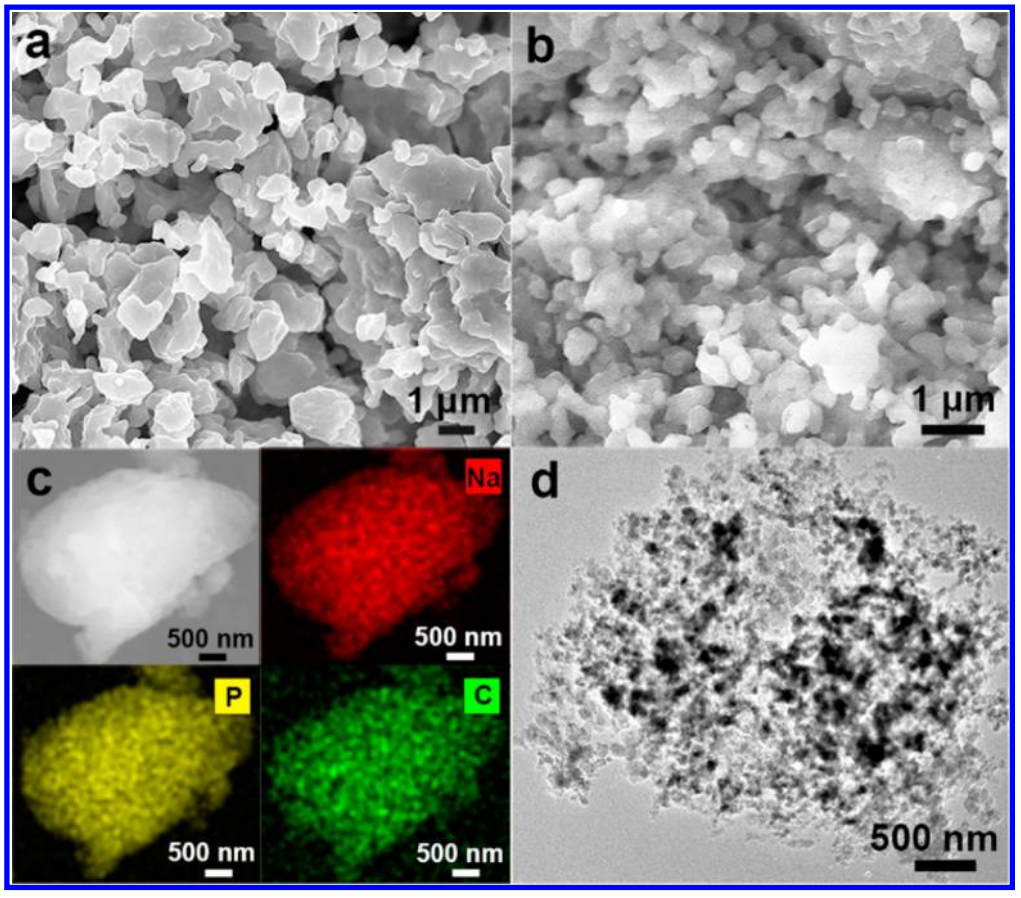

Figure 2. SEM images of NPS (a) and nanosized Na_2S (b). (c) SEM image and elemental mappings of sodium, phosphorus, and carbon as well as (d) TEM image for the NPS-nano-Na_2S−C nanocomposite cathode.

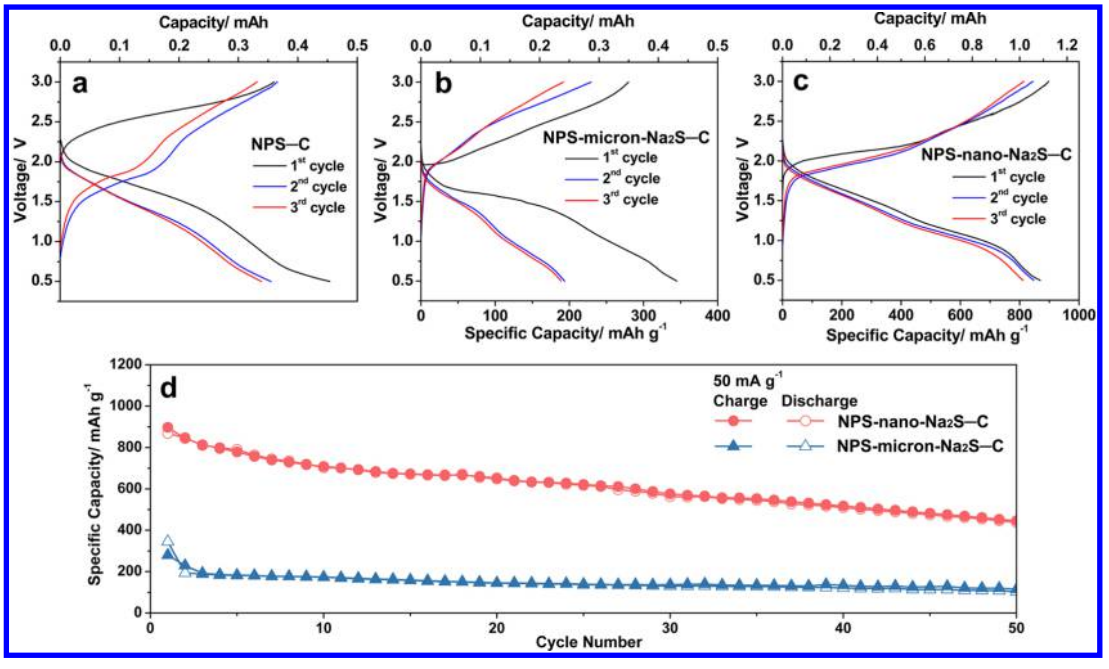

Figure 3. Electrochemical performances of the NPS−C catholyte, NPS-micron-Na_2S−C composite, and NPS-nano-Na_2S−C nanocomposite cathodes in ASSB tested at 60 °C between 0.5 and 3 V. First three charge−discharge curves of NPS−C catholyte (a), NPS-micron-Na_2S−C composite (b), and NPS-nano-Na_2S−C nanocomposite (c) cathodes at 50 mA g^{-1}. The upper axis shows the total capacity of the electrode composite, and the lower axis shows the specific capacities based on the weight of Na_2S in the composite electrode. (d) Cycling performance of NPS-micron-Na_2S−C composite and NPS-nano-Na_2S−C nanocomposite cathodes at a current of 50 mA g^{-1}. All of the current densities were calculated based on the weight of Na_2S in the composite electrodes.

DOI: 10.1021/acsnano.7b01445
ACS Nano 2017, 11, 4885−4891

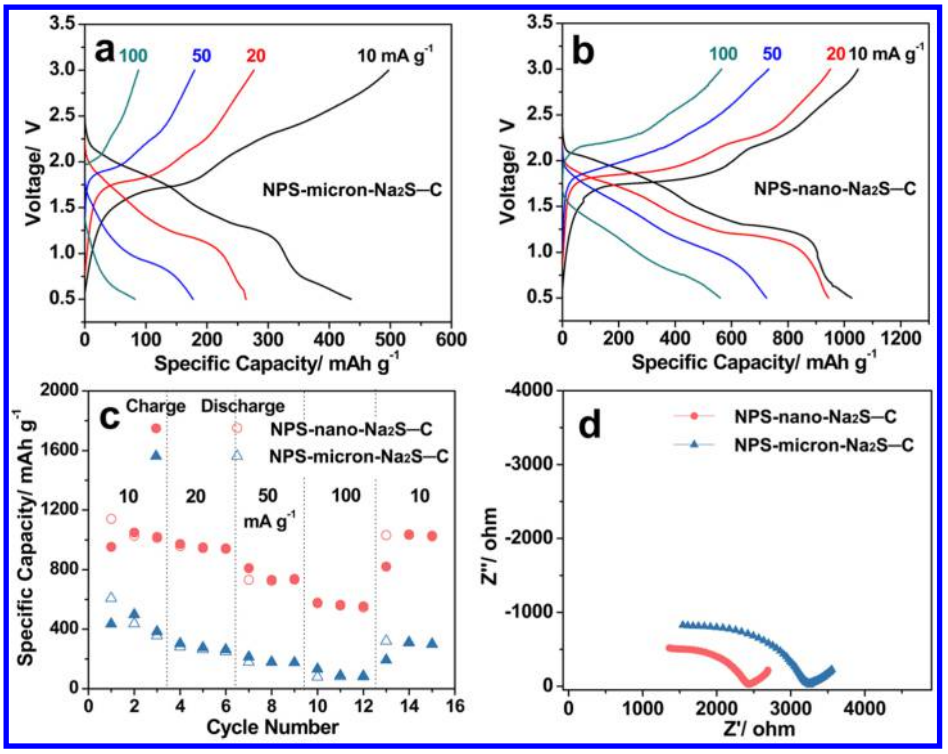

Figure 4. Charge–discharge profiles of the NPS-micron-Na_2S–C composite (a) and NPS-nano-Na_2S–C nanocomposite cathodes (b) in the ASSB at 60 °C between 0.5 and 3 V at various current densities from 10 to 100 mA g^{-1}. The cells were discharged and charged for three cycles at each current density, and the second charge–discharge profiles were provided. (c) Rate performance of the NPS-micron-Na_2S–C composite and NPS-nano-Na_2S–C nanocomposite cathodes in the ASSB at 60 °C between 0.5 and 3 V. (d) Impedance profiles the ASSBs using NPS-micron-Na_2S–C composite and NPS-nano-Na_2S–C nanocomposite cathodes. The EIS was tested at the fully discharged state of the batteries.

nonuniform distribution of micron-sized Na_2S, Na_3PS_4, and carbon in the NPS-micron-Na_2S–C composite.

The electrochemical performances of the NPS–C catholyte, NPS-micron-Na_2S–C composite, and NPS-nano-Na_2S–C nanocomposite cathodes were tested in the ASSB using cubic Na_3PS_4 as solid electrolyte and Na–Sn–C composite as the anode in a voltage range of 0.5–3.0 V at 60 °C. The thicknesses of the solid electrolyte and cathode composite are approximately 1 mm and 15 μm, respectively, as determined from the cross-section SEM image and elemental mappings (Figure S4). Note that sodium metal was not used as anode because Na_3PS_4 solid electrolyte is not electrochemically stable with sodium metal and will be reduced to Na_2S and Na_3P after contacting with Na.[30,31] The decomposition of Na_3PS_4 at the Na/Na_3PS_4 interface will lead to a huge and continuously increased interfacial resistance.[30] Therefore, Na–Sn–C composite, which has a better interfacial stability with Na_3PS_4, was used as the anode.[20,32,33] The C (acetylene black) additive in the Na–Sn–C anodes functions as a buffer for the huge volume change of the Na–Sn anode during charge/discharge process, thus leading to a better anode/electrolyte interfacial stability during long-term charge/discharge cycles.[33] Detailed characterizations of the Na_3PS_4 solid electrolyte (Figure S5) indicate that the activation energy of Na_3PS_4 is 0.45 eV, and the ionic conductivities are 1.09×10^{-4} and 3.4×10^{-4} S cm^{-1} at 28 and 60 °C, respectively. Figure 3a shows the first three charge–discharge profiles of the NPS–C catholyte. A recent computational calculation on the electrochemical stability of Cl-doped Na_3PS_4 confirms that Na_3PS_4 will be converted into S cathode during the first charge above 2.4 V,[31] similar to the redox reaction of Li_3PS_4.[34] Therefore, the slope plateau above 2.0 V in the first charge process could be attributed to the oxidation of S^{2-} contained in Na_3PS_4.[31] The first discharge curve shows a large plateau at 1.6 V that can be ascribed to the reduction of S, followed by several small plateaus, which might be caused by the reduction of P contained in the Na_3PS_4 solid electrolyte.[31] Highly reversible charge/discharge process could be observed in the following cycles, indicating that Na_3PS_4 electrolyte could also function as an electrode after mixing with electronic conductive carbon. The total capacity of the NPS–C catholyte (the weight of Na_3PS_4 in the cathode is 2.5 mg) is around 0.35 mAh. Figure 3b shows the first charge/discharge profiles of the NPS-micron-Na_2S–C composite cathode. Similar charge/discharge curves can be observed as the NPS–C catholyte. However, the total capacity of the NPS-micron-Na_2S–C composite cathode is even lower than that of the NPS–C catholyte, although microsized Na_2S was added. This is because Na_2S has very low electronic and ionic conductivities, and microsized Na_2S particles may actually block the transport path of both Na^+ and electrons in the cathode, leading to the capacity loss of Na_3PS_4. On the other hand, the NPS-nano-Na_2S–C nanocomposite cathode with the addition of nanosized Na_2S exhibits a significantly improved electrochemical performance (Figure 3c). A much smaller voltage hysteresis with a higher reversibility can be observed during the charge/discharge process, confirming the enhanced reaction kinetics due to the homogeneous distribution of nanosized Na_3PS_4, nanosized Na_2S, and nanosized carbon in the NPS-nano-Na_2S–C nanocomposite cathode. Moreover, the first total capacity of the NPS-nano-Na_2S–C nanocomposite cathode was increased to over 1.1 mAh, which is three times the capacity of NPS–C catholyte. The NPS-nano-Na_2S–C nanocomposite cathode

DOI: 10.1021/acsnano.7b01445
ACS Nano 2017, 11, 4885–4891

could maintain much higher total capacity than the NPS−C catholyte for 50 cycles (Figure S6). In addition, the Coulombic efficiency of the NPS-nano-Na_2S−C nanocomposite cathode (Figure 3c) was also significantly enhanced compared with that of the NPS−C catholyte (Figure 3a). It should be noted that the achieved capacities are even larger than the theoretical capacity of Na_2S (687 mAh g^{-1}), which also confirms that the reversible decompositions of Na_3PS_4 contribute to the capacity of the electrode.[35] Figure 3d presents the cycling performances of the NPS-micron-Na_2S−C and NPS-nano-Na_2S−C composite cathodes at 50 mA g^{-1}. The NPS-nano-Na_2S−C nanocomposite cathode exhibits a reversible capacity of 438.4 mAh g^{-1} after 50 cycles, which is much higher than that of NPS-micron-Na_2S−C composite cathode (103 mAh g^{-1}). It should be noted that the electrochemical performance of the all-inorganic solid-state sodium−sulfur battery using the NPS-nano-Na_2S−C composite cathode is much better than that of the polymer electrolyte sodium−sulfur batteries, which only exhibit low capacities with limited cycling performance (<10 cycles).[13,14] In addition, the electrochemical performances of the NPS-nano-Na_2S−C cathodes with higher contents of nanosized Na_2S were also investigated. Figure S7 shows the cycling performances of the NPS-nano-Na_2S−C cathodes with the weight ratio of 2:2:1 and 2:3:1. Both of these cathodes delivered a higher total capacity for the first few cycles than the NPS-nano-Na_2S−C cathode with the weight ratio of 2:1:1. However, these two cathodes suffered from poor capacity stability. After 50 cycles, the total capacity of these cathodes dropped to around 0.4−0.5 mAh, which is lower than that of the cathode with a weight ratio of 2:1:1 (0.55 mAh). Moreover, the specific capacity based on the weight of Na_2S also decreased for these cathodes, indicating a lower utilization of Na_2S. The poor performances of the cathodes with high contents of Na_2S are caused by the decrease of ionic/electronic conductivity and the increase of the volume change of the cathode composite. Therefore, NPS-nano-Na_2S−C with a weight ratio of 2:1:1 was used in this work.

The rate capabilities of the NPS-micron-Na_2S−C composite and NPS-nano-Na_2S−C nanocomposite cathodes were also tested at 60 °C by increasing the current density from 10 to 100 mA g^{-1}. As shown in Figure 4a, the specific capacity of the NPS-micron-Na_2S−C composite cathode quickly decreases with the increase of the current density. The specific capacities of the NPS-micron-Na_2S−C composite cathode at 10, 20, 50, and 100 mA g^{-1} are 448, 261, 182, and 85 mAh g^{-1}. However, the NPS-nano-Na_2S−C nanocomposite cathode could deliver a much higher capacity of 1026, 944, 724, and 559 mAh g^{-1} at 10, 20, 50, and 100 mA g^{-1} (Figure 4b), respectively. Moreover, the capacity could increase back to 1030 mAh g^{-1} when the current decreased back to 10 mA g^{-1}, indicating great stability of the NPS-nano-Na_2S−C nanocomposite cathode during high-rate charge/discharge processes (Figure 4c). To gain insights into the mechanism for the huge difference between the NPS-micron-Na_2S−C composite and NPS-nano-Na_2S−C nanocomposite cathodes, electrochemical impedance spectra (EIS) of the ASSBs using these two cathodes were measured (Figure 4d). The EIS of both cells were tested at fully discharged state after resting at open-circuit potential for 2 h. The observed semicircles in the EIS spectra represent the interfacial resistances, whereas the slope line in the low-frequency region is due to the Na^+ diffusion in the cathodes. NPS-nano-Na_2S−C nanocomposite cathode exhibits an interfacial resistance much lower than that of the NPS-micron-Na_2S−C composite cathode. The largely decreased cathode/electrolyte interfacial resistance benefits from the homogeneous distribution of nanosized Na_2S, Na_3PS_4, and carbon in the NPS-nano-Na_2S−C nanocomposite cathode, which eventually leads to the significantly improved electrochemical performances.

In addition, the degradation mechanism of the ASSB with the NPS-nano-Na_2S−C cathode was also investigated. Figure 5 shows the impedance profiles of the ASSB using NPS-nano-Na_2S−C as the cathode at different cycles. The result shows the interfacial resistance within the battery continuously increases during charge/discharge cycles. The continuously increased interfacial resistance is probably attributed to the mechanical degradation of the cathode, which is induced by accumulated strain/stress from the huge volume change of the electrode during charge/discharge processes. It should be noted that the continuous increase of the interfacial resistance with charge/discharge cycles in the ASSB with the NPS-micron-Na_2S−C cathode was also observed (Figure S8). We believe further improvements of the battery performance could still be possible by stabilizing the interfacial resistance during long-term charge/discharge cycles through optimizing the cathode structure.

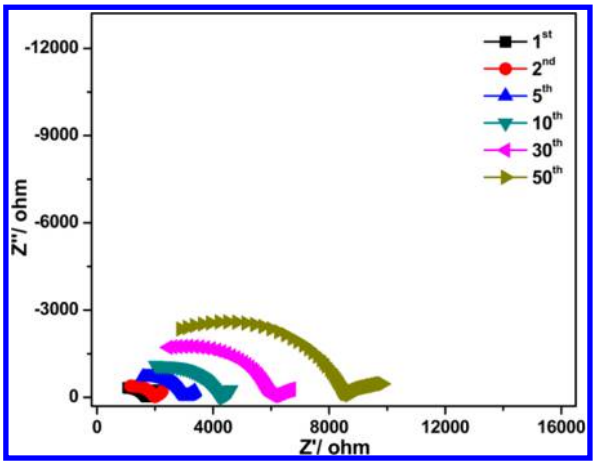

Figure 5. Impedance profiles of the ASSB using NPS-nano-Na_2S−C nanocomposite cathode at different cycles.

The development of high-performance ASSB is really challenging due to the large interfacial resistance arising from the insufficient triple-phase contact of sulfur active material with both solid electrolyte and carbon. By using highly ionic conductive Na_3PS_4 as both electrolyte and electrode, the interfacial resistance was significantly reduced. The addition of Na_2S into Na_3PS_4 could largely increase the capacity of the electrode only if the particle size of Na_2S was reduced to nanometer scale. Sufficient triple-phase contact of nanosized active material, ionic conductive solid electrolyte, and electronic conductive carbon could be achieved in the NPS-nano-Na_2S−C nanocomposite cathode. The nanosized Na_3PS_4 and Na_2S active materials could also shorten the diffusion paths for both Na^+ and electrons, which will help to increase the utilization of the active material during charge and discharge. In addition, utilization of the presodiated sulfides as active material could provide enough space for the volume change of the solid electrode during charge/discharge. All of these properties of the NPS-nano-Na_2S−C nanocomposite cathode make it a promising candidate for high-performance ASSBs.

DOI: 10.1021/acsnano.7b01445
ACS Nano 2017, 11, 4885−4891

CONCLUSIONS

In summary, a Na_3PS_4−Na_2S−C nanocomposite was proposed as an innovative cathode for all-inorganic solid-state sodium−sulfur batteries. Highly ionic conductive Na_3PS_4 could function as both solid electrolyte and active material after mixing with carbon, leading to an intrinsic superior interfacial contact because only a two-phase contact is required for charge transfer reaction. A 2-fold increase of the capacity could be achieved after introducing nanosized Na_2S into Na_3PS_4−C to make the Na_3PS_4−Na_2S−C nanocomposite cathode. The homogeneous distribution of nanosized Na_3PS_4, nanosized Na_2S, and nanosized carbon in the Na_3PS_4−Na_2S−C nanocomposite cathode could ensure a sufficient interfacial contact and high mixed (ionic and electronic) conductivities. The all-inorganic solid-state sodium−sulfur battery using such a nanocomposite cathode could deliver a high reversible capacity of 869.2 mAh g^{-1} with an excellent cycling (438.4 mAh g^{-1} after 50 cycles at 50 mA g^{-1}) and rate capabilities at 60 °C in the all-inorganic solid-state sodium−sulfur battery, representing the best performance of all-solid-state sodium−sulfur batteries reported to date. The proposed electrode design could promote the practical applications of the safe, high-energy all-inorganic solid-state sodium−sulfur batteries and may be also applied to other all-solid-state energy storage systems.

METHODS

Sample Synthesis. Na_3PS_4 solid electrolyte was prepared *via* a mechanical milling method followed by an annealing process, based on a previous report.[36] In brief, a mixture of 75 mol % of sodium sulfide (Na_2S, Sigma-Aldrich) and 25 mol % of phosphorus pentasulfide (P_2S_5, Sigma-Aldrich) was milled in a zirconia (ZrO_2) pot with the volume of 50 mL, at a fixed rotation speed of 510 rpm for 20 h. The obtained powder was then heated at 270 °C for 1 h in Ar. The Na_3PS_4−Na_2S−C composite cathodes were prepared by mechanical milling of Na_3PS_4, nanosized Na_2S (or commercial micron-sized Na_2S), and acetylene black (Soltex, Inc.) with the weight ratio of 50:25:25 in a stainless steel pot with volume of 50 mL at 370 rpm for 1 h. The nanosized Na_2S was prepared by ball-milling the commercial micron-sized Na_2S at a rotation speed of 510 rpm for 20 h. The Na_3PS_4−C catholyte was prepared by ball-milling Na_3PS_4 with acetylene black with a weight ratio of 50:25 in a stainless steel pot with volume of 50 mL at 370 rpm for 1 h. All these processes were performed under argon atmosphere.

Material Characterization. XRD patterns were recorded on a D8 Advance X-ray diffractometer (Bruker AXS, WI, USA) with Cu Kα line as a radiation source. SEM images were observed on a Hitachi SU-70 field emission scanning electron microscope. TEM images were achieved on a field emission transmission electron microscope (JEOL 2100F).

Electrochemical Measurement. The ionic conductivities of Na_3PS_4 solid electrolyte were measured by EIS using an ion-blocking Pt/Na_3PS_4/Pt cell prepared by cold pressing of 150 mg of Na_3PS_4, followed by Pt sputtering. The all-inorganic solid-state sodium−sulfur batteries were fabricated using the as-obtained composite as working electrode, Na_3PS_4 as the solid electrolyte, and a Na−Sn−C composite as the counter as well as reference electrodes. The Na−Sn−C composite was prepared according to a reported method.[36] To assemble the cell, the Na_3PS_4−Na_2S−C powder (5 mg) or Na_3PS_4−C powder (3.75 mg) composite cathodes were put on one side of the Na_3PS_4 solid electrolyte (120 mg) in a PTFE tank with a diameter of 10 mm, and Na−Sn−C anode powders (100 mg) were placed on the other side of the solid electrolyte membrane and then cold-pressed together under 360 MPa between two stainless steel rods, which act as the current collectors. Galvanostatic discharge−charge cycles were conducted using a battery cycler (LAND CT-2001A, China) in a voltage of 0.5−3.0 V at 60 °C. The current densities and specific capacities in this report were calculated based on the weight of Na_2S. EIS were obtained by an electrochemistry workstation (Solatron 1287/1260) over a frequency range from 1 MHz to 0.1 Hz, with an AC amplitude of 20 mV.

ASSOCIATED CONTENT

Supporting Information

The Supporting Information is available free of charge on the ACS Publications website at DOI: 10.1021/acsnano.7b01445.

Characterizations of the Na_3PS_4−C composite, Na_3PS_4 micron-sized Na_2S−C composite, and Na_3PS_4 solid electrolyte with cathode composite; XRD patterns of Na_2S; Arrhenius plot, and the corresponding EIS spectra of the Na_3PS_4 electrolyte; cycling performances of the composite cathodes at 60 °C; impedance profiles of the ASSB using NPS-micron-Na_2S−C composite cathode at different cycles (PDF)

AUTHOR INFORMATION

Corresponding Authors

*E-mail: yangjian@sdu.edu.cn.
*E-mail: cswang@umd.edu.

ORCID

Jian Yang: 0000-0002-6401-276X
Chunsheng Wang: 0000-0002-8626-6381

Author Contributions

J.Y. and F.H. contributed equally to this work.

Notes

The authors declare no competing financial interest.

ACKNOWLEDGMENTS

This work was supported by Army Research Office (Program Manager: Dr. Robert Mantz) under Award No. W911NF1510187. J.Y. was also supported by China Scholarship Council (CSC) (File No. 201506220050). F.H. thanks the support from the Harry K. Wells Fellowship.

REFERENCES

(1) Wei, S. Y.; Xu, S. M.; Agrawral, A.; Choudhury, S.; Lu, Y. Y.; Tu, Z. Y.; Ma, L.; Archer, L. A. A Stable Room-Temperature Sodium-Sulfur Battery. *Nat. Commun.* **2016**, *7*, 11722.

(2) Wen, Z. Y.; Hu, Y. Y.; Wu, X. W.; Han, J. D.; Gu, Z. H. Main Challenges for High Performance NAS Battery: Materials and Interfaces. *Adv. Funct. Mater.* **2013**, *23*, 1005−1018.

(3) Kummer, J. T.; Weber, N. Sodium-Sulfur Secondary Battery. *SAE Trans.* **1968**, *76*, 88−99.

(4) Lu, X. C.; Xia, G. G.; Lemmon, J. P.; Yang, Z. G. Advanced Materials for Sodium-beta Alumina Batteries: Status, Challenges and Perspectives. *J. Power Sources* **2010**, *195*, 2431−2442.

(5) Wenzel, S.; Metelmann, H.; Raiß, C.; Dürr, A. K.; Janek, J.; Adelhelm, P. Thermodynamics and Cell Chemistry of Room Temperature Sodium/Sulfur Cells with Liquid and Liquid/Solid Electrolyte. *J. Power Sources* **2013**, *243*, 758−765.

(6) Yu, X. W.; Manthiram, A. Performance Enhancement and Mechanistic Studies of Room-Temperature Sodium−Sulfur Batteries with a Carbon-Coated Functional Nafion Separator and a Na_2S/Activated Carbon Nanofiber Cathode. *Chem. Mater.* **2016**, *28*, 896−905.

(7) Xin, S.; Yin, Y. X.; Guo, Y. G.; Wan, L. J. A High-Energy Room-Temperature Sodium-Sulfur Battery. *Adv. Mater.* **2014**, *26*, 1261−1265.

(8) Kohl, M.; Borrmann, F.; Althues, H.; Kaskel, S. Hard Carbon Anodes and Novel Electrolytes for Long-Cycle-Life Room Temper-

DOI: 10.1021/acsnano.7b01445
ACS Nano 2017, 11, 4885−4891

ature Sodium-Sulfur Full Cell Batteries. *Adv. Energy Mater.* **2016**, *6*, 1502185.
(9) Lee, D. J.; Park, J. W.; Hasa, I.; Sun, Y. K.; Scrosati, B.; Hassoun, J. Alternative Materials for Sodium Ion-Sulphur Batteries. *J. Mater. Chem. A* **2013**, *1*, 5256−5261.
(10) Wang, J. L.; Yang, J.; Nuli, Y.; Holze, R. Room Temperature Na/S Batteries with Sulfur Composite Cathode Materials. *Electrochem. Commun.* **2007**, *9*, 31−34.
(11) Hwang, T. H.; Jung, D. S.; Kim, J. S.; Kim, B. G.; Choi, J. W. One-Dimensional Carbon-Sulfur Composite Fibers for Na-S Rechargeable Batteries Operating at Room Temperature. *Nano Lett.* **2013**, *13*, 4532−4538.
(12) Kim, I.; Park, J. Y.; Kim, C. H.; Park, J. W.; Ahn, J. P.; Ahn, J. H.; Kim, K. W.; Ahn, H. J. A Room Temperature Na/S Battery Using a β'' Alumina Solid Electrolyte Separator, Tetraethylene Glycol Dimethyl Ether Electrolyte, and a S/C Composite Cathode. *J. Power Sources* **2016**, *301*, 332−337.
(13) Park, C. W.; Ryu, H. S.; Kim, K. W.; Ahn, J. H.; Lee, J. Y.; Ahn, H. J. Discharge Properties of All-Solid Sodium-Sulfur Battery Using Poly (Ethylene Oxide) Electrolyte. *J. Power Sources* **2007**, *165*, 450−454.
(14) Park, C. W.; Ahn, J. H.; Ryu, H. S.; Kim, K. W.; Ahn, H. J. Room-Temperature Solid-State Sodium/Sulfur Battery. *Electrochem. Solid-State Lett.* **2006**, *9*, A123−A125.
(15) Hu, Y. S. Batteries: Getting Solid. *Nat. Energy* **2016**, *1*, 16042.
(16) Janek, J.; Zeier, W. G. A Solid Future for Battery Development. *Nat. Energy* **2016**, *1*, 16141.
(17) Mikhaylik, Y. V.; Akridge, J. R. Polysulfide Shuttle Study in the Li/S Battery System. *J. Electrochem. Soc.* **2004**, *151*, A1969−A1976.
(18) Tikekar, M. D.; Choudhury, S.; Tu, Z.; Archer, L. A. Design Principles for Electrolytes and Interfaces for Stable Lithium-Metal Batteries. *Nat. Energy* **2016**, *1*, 16114.
(19) Han, F. D.; Yue, J.; Fan, X. L.; Gao, T.; Luo, C.; Ma, Z. H.; Suo, L. M.; Wang, C. S. High-Performance All-Solid-State Lithium-Sulfur Battery Enabled by a Mixed-Conductive Li_2S Nanocomposite. *Nano Lett.* **2016**, *16*, 4521−4527.
(20) Nagata, H.; Chikusa, Y. An All-Solid-State Sodium-Sulfur Battery Operating at Room Temperature Using a High-Sulfur-Content Positive Composite Electrode. *Chem. Lett.* **2014**, *43*, 1333−1334.
(21) Yang, Y.; Yu, G. H.; Cha, J. J.; Wu, H.; Vosgueritchian, M.; Yao, Y.; Bao, Z. N.; Cui, Y. Improving the Performance of Lithium-Sulfur Batteries by Conductive Polymer Coating. *ACS Nano* **2011**, *5*, 9187−9193.
(22) Zhou, G. M.; Yin, L. C.; Wang, D. W.; Li, L.; Pei, S. F.; Gentle, I. R.; Li, F.; Cheng, H. M. Fibrous Hybrid of Graphene and Sulfur Nanocrystals for High-Performance Lithium-Sulfur Batteries. *ACS Nano* **2013**, *7*, 5367−5375.
(23) Zhou, W. D.; Chen, H.; Yu, Y. C.; Wang, D. L.; Cui, Z. M.; DiSalvo, F. J.; Abruna, H. D. Amylopectin Wrapped Graphene Oxide/Sulfur for Improved Cyclability of Lithium-Sulfur Battery. *ACS Nano* **2013**, *7*, 8801−8808.
(24) Lin, Z.; Liu, Z. C.; Dudney, N. J.; Liang, C. D. Lithium Superionic Sulfide Cathode for All-Solid Lithium-Sulfur Batteries. *ACS Nano* **2013**, *7*, 2829−2833.
(25) Lin, Z.; Liu, Z. C.; Fu, W. J.; Dudney, N. J.; Liang, C. D. Lithium Polysulfidophosphates: A Family of Lithium-Conducting Sulfur-Rich Compounds for Lithium-Sulfur Batteries. *Angew. Chem.* **2013**, *125*, 7608−7611.
(26) Han, F. D.; Gao, T.; Zhu, Y. J.; Gaskell, K. J.; Wang, C. S. A Battery Made from a Single Material. *Adv. Mater.* **2015**, *27*, 3473−3483.
(27) Yue, J.; Wang, W. P.; Wang, N. N.; Yang, X. F.; Feng, J. K.; Yang, J.; Qian, Y. T. Triple-Walled SnO_2@N-doped Carbon@SnO_2 Nanotubes as an Advanced Anode Material for Lithium and Sodium Storage. *J. Mater. Chem. A* **2015**, *3*, 23194−23200.
(28) Nagao, M.; Hayashi, A.; Tatsumisago, M.; Ichinose, T.; Ozaki, T.; Togawa, Y.; Mori, S. Li_2S Nanocomposites Underlying High-Capacity and Cycling Stability in All-Solid-State Lithium-Sulfur Batteries. *J. Power Sources* **2015**, *274*, 471−476.
(29) Nagao, M.; Hayashi, A.; Tatsumisago, M. High-Capacity Li_2S-Nanocarbon Composite Electrode for All-Solid-State Rechargeable Lithium Batteries. *J. Mater. Chem.* **2012**, *22*, 10015−10020.
(30) Wenzel, S.; Leichtweiss, T.; Weber, D. A.; Sann, J.; Zeier, W. G.; Janek, J. Interfacial Reactivity Benchmarking of the Sodium Ion Conductors Na_3PS_4 and Sodium β-Alumina for Protected Sodium Metal Anodes and Sodium All-Solid-State Batteries. *ACS Appl. Mater. Interfaces* **2016**, *8*, 28216−28224.
(31) Chu, I. H.; Kompella, C. S.; Nguyen, H.; Zhu, Z. Y.; Hy, S.; Deng, Z.; Meng, Y. S.; Ong, S. P. Room-Temperature All-solid-state Rechargeable Sodium-ion Batteries with a Cl-doped Na_3PS_4 Superionic Conductor. *Sci. Rep.* **2016**, *6*, 33733.
(32) Hayashi, A.; Noi, K.; Sakuda, A.; Tatsumisago, M. Superionic Glass-Ceramic Electrolytes for Room-Temperature Rechargeable Sodium Batteries. *Nat. Commun.* **2012**, *3*, 856.
(33) Tanibata, N.; Hayashi, A.; Tatsumisago, M. Improvement of Rate Performance for All-Solid-State $Na_{15}Sn_4$/Amorphous TiS_3 Cells Using $94Na_3PS_4{\cdot}6Na_4SiS_4$ Glass-Ceramic Electrolytes. *J. Electrochem. Soc.* **2015**, *162*, A793−A795.
(34) Zhu, Y. Z.; He, X. F.; Mo, Y. F. Origin of Outstanding Stability in the Lithium Solid Electrolyte Materials: Insights from Thermodynamic Analyses Based on First-Principles Calculations. *ACS Appl. Mater. Interfaces* **2015**, *7*, 23685−23693.
(35) Han, F. D.; Zhu, Y. Z.; He, X. F.; Mo, Y. F.; Wang, C. S. Electrochemical Stability of $Li_{10}GeP_2S_{12}$ and $Li_7La_3Zr_2O_{12}$ Solid Electrolytes. *Adv. Energy Mater.* **2016**, *6*, 1501590.
(36) Hayashi, A.; Noi, K.; Tanibata, N.; Nagao, M.; Tatsumisago, M. High Sodium Ion Conductivity of Glass Ceramic Electrolytes with Cubic Na_3PS_4. *J. Power Sources* **2014**, *258*, 420−423.

DOI: 10.1021/acsnano.7b01445
ACS Nano 2017, 11, 4885−4891